

# Nonadiabatic electromigration along a one-dimensional gold chain

Masaaki Araidai\* and Masaru Tsukada†

WPI Advanced Institute for Materials Research, Tohoku University, 2-1-1 Katahira, Aoba-ku, Sendai, Miyagi 980-8577, Japan  
 CREST, Japan Science and Technology Agency, 4-1-8 Honcho Kawaguchi, Saitama 332-0012, Japan

(Received 15 May 2011; revised manuscript received 9 November 2011; published 28 November 2011)

We have investigated nonadiabatic processes of electromigration by theoretical calculation, taking the example of a gold atom moving along a chain of gold atoms. The calculated electromigration rate showed almost linear behavior beyond a threshold and rapidly increased with increasing applied bias voltage. It was found from the detailed analysis that the electronic scattering takes place via the  $d$  orbitals of a migrating Au atom with larger lobes in the migration direction, accompanied by an excitation of the atom vibration from the ground state to a continuum state, leading to nonadiabatic electromigration. Through a comparison of the electromigration rates between nonadiabatic and thermal migration, we clarified that the nonadiabatic contribution is dominant at low temperature and low bias beyond the threshold voltage.

DOI: 10.1103/PhysRevB.84.195461

PACS number(s): 73.63.Nm, 72.10.Bg, 66.30.Qa

## I. INTRODUCTION

Electromigration is the directed migration of atoms caused by a large electric current density, and it is one of the key issues for nanoscale conductors since it is a major failure mechanism in the operation of electronic devices with a larger current density than their macroscopic counterparts. While the study has quite a long history in both experiments<sup>1-7</sup> and theoretical calculations,<sup>1,8-13</sup> the microscopic mechanisms are not yet fully understood owing to the complexities of the measurements and the underlying physics. It is commonly believed that electromigration is driven by electrostatic forces, momentum transfers by electrons to atoms (the electron wind force), and local Joule heating around migrating atoms to facilitate the atomic diffusion. There are many theoretical studies about the above driving forces within the adiabatic approximation which makes the problem tractable. Previously, the present authors also investigated single-atom electromigration along a chain of gold atoms by first-principles calculations within the adiabatic approximation from the viewpoint of atomic diffusion processes.<sup>13</sup> In the study, the potential-energy surfaces of the migrating atom under applied bias voltages were calculated, the migration pathway (oscillating curve in the top panel of Fig. 1) was determined as a valley of the potential-energy surface, and the electromigration rate on the pathway was evaluated from the potential-energy curve to estimate the local temperature around the migrating gold atom.

Recently, two groups reported the elemental process of electromigration within the ballistic regime.<sup>4,6</sup> Wu *et al.* performed four-terminal measurements for electromigration at gold nanojunctions and found that the junction resistance depends only slightly on temperature.<sup>4</sup> Umeno and Hirakawa performed a feedback-controlled break junction process at gold nanojunctions to fabricate nanogap electrodes and observed a decrease of critical power dissipation causing initiation of electromigration at the junctions.<sup>6</sup> The remarkable point from both experiments is that the origin of electromigration at gold junctions is nonthermal within the ballistic regime. This implies that additional contributions beyond the adiabatic approximation are essential to clarify the migration mechanisms within the ballistic regime. Accordingly, in this study, we calculate the nonadiabatic contributions to the

electromigration rate with the same model as in the previous study,<sup>13</sup> and discuss whether the non-adiabatic contributions are dominant compared with the thermal ones.

The arrangement of this paper is as follows. In Sec. II, we elaborate on our theoretical model of nonadiabatic electromigration. Several numerical results of single-atom electromigration along a gold chain, using the model, are presented in Sec. III. We compare the features and importance of the nonadiabatic contribution with those of the thermal one in Sec. IV. Section V is devoted to a summary and outlook.

## II. THEORETICAL MODEL

### A. Mathematical formulation

The nonadiabatic process we assumed is as follows: A gold atom is occasionally kicked out from the local potential well by ballistic electrons, and migrates in the descending direction of the overall potential. The Au atom is kicked out by a stimulation due to a quantum transition of an electron from an initial higher to a final lower ballistic state accompanied by an excitation of the Au atom vibration from the ground state  $\Phi_{\varepsilon_0}(\mathbf{R})$  to a continuum state  $\Phi_{\varepsilon}(\mathbf{R})$  above the barrier. Figure 1 shows a schematic diagram of the electromigration of a single gold atom along a one-dimensional gold chain within the nonadiabatic process. The excitation rate per unit of time is given by the following equation:

$$\Gamma(V) = \frac{2\pi}{\hbar} \sum_{k,i} \sum_{k',i'} \int d\varepsilon |\gamma_{k',i' \leftarrow k,i}^{\varepsilon \leftarrow \varepsilon_0}|^2 \times [f(E_{k,i}) - f(E_{k',i'} + eV)] \times \delta(E_{k',i'} + \varepsilon - (E_{k,i} + \varepsilon_0)). \quad (1)$$

In the above,  $f(E)$  is the Fermi-Dirac distribution function of electrons,  $E_{k,i}$  and  $E_{k',i'}$  are the electron energies of the initial and final states, and  $\gamma_{k',i' \leftarrow k,i}^{\varepsilon \leftarrow \varepsilon_0}$  is the matrix element between the initial and final states of the transition,  $[\Psi_{E_{k',i'}}(\mathbf{r}), \Phi_{\varepsilon}(\mathbf{R}) \leftarrow \Psi_{E_{k,i}}(\mathbf{r}), \Phi_{\varepsilon_0}(\mathbf{R})]$ ,

$$\gamma_{k',i' \leftarrow k,i}^{\varepsilon \leftarrow \varepsilon_0} = \int d\mathbf{r} \Psi_{E_{k',i'}}^*(\mathbf{r}) \Psi_{E_{k,i}}(\mathbf{r}) W_{\varepsilon \leftarrow \varepsilon_0}(\mathbf{r}). \quad (2)$$

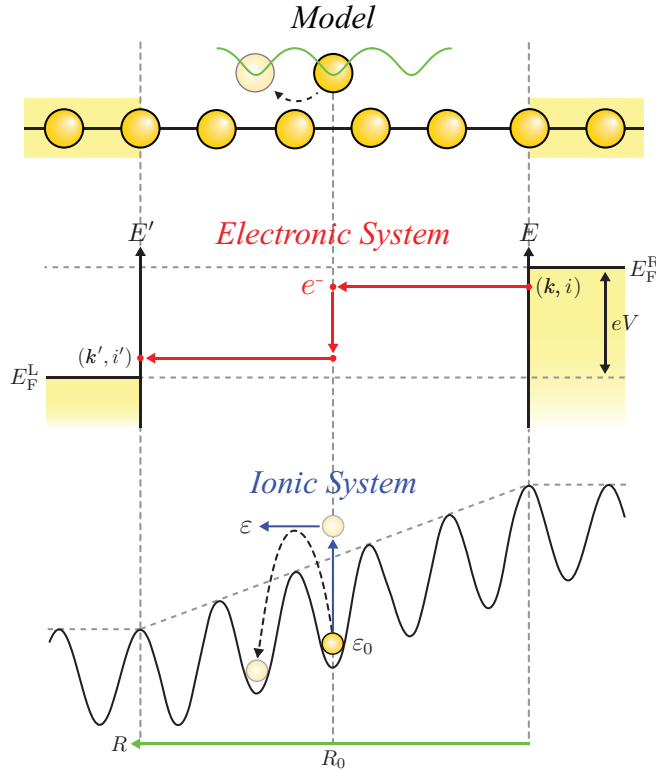


FIG. 1. (Color online) Schematic diagram of nonadiabatic electromigration. The top panel shows the calculation model. Note that the actually calculated number of gold atoms in the straight chain is 14 and is the same as in Ref. 13. The green (oscillating) curve is the migration pathway. The middle and bottom panels are energy diagrams of the electronic and ionic systems. An electronic state  $\Psi_{E_{k,i}}$  comes into the scattering region from the right electrode, it is scattered by the migrating atom with (without) the ionic excitation from the ground  $\Phi_{\varepsilon_0}$  to continuum  $\Phi_{\varepsilon}$  states, and goes out to a state  $\Psi_{E_{k',i'}}$  in the left electrode with (without) energy loss. The oscillating curve in the bottom panel is the adiabatic potential-energy curve of the migrating atom on the pathway subject to an applied bias voltage. In the adiabatic case, the atom is confined in the potential and cannot migrate without sufficient thermal energy.

In Eq. (2),  $\Psi_E(\mathbf{r})$  is an electron wave function with energy  $E$  and  $W_{\varepsilon \leftarrow \varepsilon_0}(\mathbf{r})$  is the scattering potential for electronic transitions,

$$W_{\varepsilon \leftarrow \varepsilon_0}(\mathbf{r}) = \int d\mathbf{R} \Phi_{\varepsilon}^*(\mathbf{R}) \Phi_{\varepsilon_0}(\mathbf{R}) \times [V(\mathbf{r} - \mathbf{R}) - V(\mathbf{r} - \mathbf{R}_0)], \quad (3)$$

where  $\mathbf{R}_0$  is the most stable position of the migrating atom and  $V(\mathbf{r})$  is an individual atomic potential. After some mathematical manipulations, we can rewrite Eq. (1) using the Green function of the electron as

$$\Gamma(V) = \frac{4}{h} \iiint dE d\varepsilon d\mathbf{r} d\mathbf{r}' \text{Im}[G^*(\mathbf{r}, \mathbf{r}'; E)] W_{\varepsilon \leftarrow \varepsilon_0}^*(\mathbf{r}) \times \text{Im}[G(\mathbf{r}, \mathbf{r}'; E + \varepsilon_0 - \varepsilon)] W_{\varepsilon \leftarrow \varepsilon_0}(\mathbf{r}') \times [f(E) - f(E + \varepsilon_0 - \varepsilon + eV)]. \quad (4)$$

If the Green function is expanded using atomic basis functions  $\varphi_{\mu}(\mathbf{r})$ , then Eq. (4) can be reduced to the matrix representation as

$$\Gamma(V) = \frac{4}{h} \iint dE d\varepsilon \text{Tr}[\text{Im}[\mathbf{G}^\dagger(E)] \mathbf{W}^\dagger(\varepsilon) \times \text{Im}[\mathbf{G}(E + \varepsilon_0 - \varepsilon)] \mathbf{W}(\varepsilon) \times [f(E) - f(E + \varepsilon_0 - \varepsilon + eV)], \quad (5)$$

where  $\mathbf{G}(E)$  is the matrix of  $G(\mathbf{r}, \mathbf{r}'; E)$  expressed via the atomic bases and  $\mathbf{W}(\varepsilon)$  is the matrix of  $W_{\varepsilon \leftarrow \varepsilon_0}(\mathbf{r})$  whose elements are defined as

$$W_{\mu\nu}(\varepsilon) = \int d\mathbf{r} \varphi_{\mu}(\mathbf{r}) \varphi_{\nu}(\mathbf{r}) W_{\varepsilon \leftarrow \varepsilon_0}(\mathbf{r}). \quad (6)$$

We considered no electronic excitation and no heat absorption in our calculations. The microscopic mechanisms for our nonadiabatic electromigration are quantum jumps. Then the electromigration should take place at a finite voltage beyond the threshold, even if the magnitude of the local electric field around the migrating atom is negligibly small or the scattering region is infinitely long. At the same time, the potential profile around the atom is also the key factor controlling the magnitude of  $\Gamma(V)$  because the details of the potential variation have a crucial influence on  $\Gamma(V)$  via  $\Phi(\mathbf{R})$ , which can be estimated from the potential.

The essential feature of the time-dependent perturbation approach is the fully quantum treatment of ionic states, and thus it is possible to capture the quantum transitions exactly. Some dynamical approaches, as in Refs. 12 and 14, also capture a part of the transitions. However, our interest in the present study is the *steady* process of atomic diffusion in electromigration, which may be detected by experiments. Then our approach would be more beneficial than the dynamical ones from the viewpoint of the computational effort. Although the difficulty of our approach is attributed to the many building blocks needing to be extracted from reliable calculations, the numerical treatment is relatively straightforward.

## B. Prescription for calculations

We use Eq. (5) to evaluate the electromigration rate as a function of applied voltage,  $\Gamma(V)$ . For the purpose, we need to obtain the matrices  $\mathbf{G}$  and  $\mathbf{W}$ . It is relatively easy to calculate the matrix  $\mathbf{G}$  because the calculation technique for the Green function is currently established. We employ the nonequilibrium Green function scheme<sup>15,16</sup> based on the self-consistent tight-binding method<sup>17</sup> to obtain the matrix  $\mathbf{G}$ . On the other hand, it is difficult to calculate the matrix  $\mathbf{W}$  owing to the quantum mechanical treatment of the ionic states. Although the ionic states<sup>18</sup>  $\Phi(\mathbf{R})$  can be evaluated from the calculated potential-energy surfaces of the migrating atom by numerical solution of the Schrödinger equation, it is computationally demanding. Accordingly, we tackle it with somewhat *ad hoc* but physically reasonable treatments as a first step.

Following our previous results, we consider that an atom migrates only along the migration pathway  $C$  on the  $x$ - $z$  plane, i.e., the plane including the Au atom chain and the adatom. Therefore the coordinate  $\mathbf{R}$  of the migrating Au atom is taken

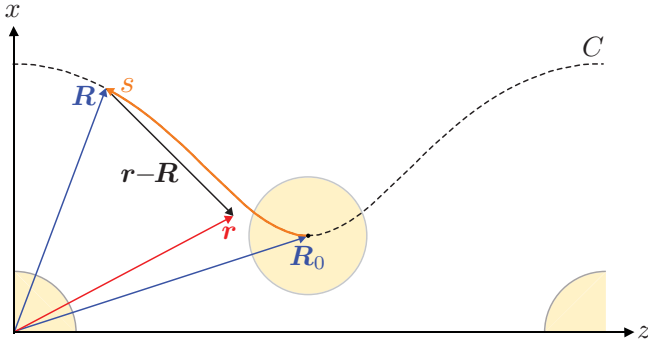


FIG. 2. (Color online) Definition of the coordinates in our calculations. The dashed curve is the electromigration pathway  $C$ . The circles are gold atoms.  $\mathbf{R}_0$  is the stable position of the migrating atom.  $s$  is the length along the pathway  $C$  from  $\mathbf{R}_0$ . The chain axis is parallel to the  $z$  direction.

as  $\mathbf{R} = (R_x, 0, R_z)$  with  $R_x$  and  $R_z$  located only on  $C$ . In this case, Eq. (3) becomes

$$W_{\varepsilon \leftarrow \varepsilon_0}(\mathbf{r}) = \int_C ds \Phi_\varepsilon^*(s) \Phi_{\varepsilon_0}(s) [V(\mathbf{r} - \mathbf{R}(s)) - V(\mathbf{r} - \mathbf{R}_0)], \quad (7)$$

where  $s$  is the coordinate on the pathway  $C$  and the origin is set to the most stable position of the migrating atom,  $\mathbf{R}_0$  [ $= \mathbf{R}(s = 0)$ ], on the pathway  $C$ , as shown in Fig. 2. The ionic wave function of the ground state  $\Phi_{\varepsilon_0}$  was simply assumed to be a Gaussian function because the potential-energy curve around the stable position of the migrating atom was well approximated as a harmonic potential. The continuum states  $\Phi_\varepsilon$  on the migration pathway can be determined from analogy with the solutions of the Schrödinger equation for a particle confined within a triangular potential, which are the Airy functions  $\text{Ai}$ . Our case corresponds to the triangular-potential case where the infinitely high barrier is positioned at  $s = -\infty$ , and the continuum states on the migration pathway were represented by Airy functions orthogonalized by the ground-state wave function. Accordingly they can be represented as<sup>18</sup>

$$\Phi_{\varepsilon_0}(s) = \left( \frac{M\omega_0}{\pi\hbar} \right)^{1/4} \exp\left[ -\frac{M\omega_0 s^2}{2\hbar} \right], \quad (8)$$

$$\Phi_\varepsilon(s) = N \left[ \text{Ai} \left( \frac{eFs - \varepsilon}{\tilde{\varepsilon}} \right) - \langle \Phi_{\varepsilon_0} | \text{Ai} \rangle \Phi_{\varepsilon_0}(s) \right], \quad (9)$$

where

$$\varepsilon_0 = \frac{1}{2}\hbar\omega_0, \quad \tilde{\varepsilon} = \left[ \frac{(eF\hbar)^2}{2m} \right]^{1/3}, \quad (10)$$

with  $M$  the atomic mass of gold.  $\varepsilon_0$  and  $F$  are the ionic ground-state energy and the global gradient of the potential experienced by the migrating atom as a function of applied bias, which were obtained in previous work. The atomic potential  $V(\mathbf{r})$  in Eq. (7) was also evaluated from *ab initio* calculations.  $N$  is the normalization constant which can be determined such that the local density of states in the zero-field limit corresponds to that of free ions, as seen in the analysis of a two-dimensional electron gas at a heterointerface.<sup>19</sup> Once  $W_{\varepsilon \leftarrow \varepsilon_0}(\mathbf{r})$  is obtained, we can evaluate the matrix  $\mathbf{W}$  from Eq. (6).

In the present study, we considered only one ionic state confined in the potential well. However, the number of ionic states in the potential well is not necessarily 1. If we take into account multiple states, then there should be some climbing up and down processes among the states. The climbing up process, however, is expected to be dominant because the energy is steadily supplied from the electron wind. Accordingly, the results with multiple states would be qualitatively the same as the present results. Also, we considered the electromigration only on the migration pathway. This approximation becomes better if the fluctuations around the migration pathway are smaller when the atom migrates along the pathway. Actually, the fluctuations can be expected to be small because the migration pathway was defined as the bottom of the valley of the potential-energy surface.

### III. NONADIABATIC ELECTROMIGRATION RATE

Figure 3(a) shows the nonadiabatic contribution to the electromigration rate of a Au atom on a Au atomic chain as a function of applied bias voltage. We immediately find from Fig. 3(a) that the calculated electromigration rate exhibits almost linear behavior beyond a specific threshold voltage

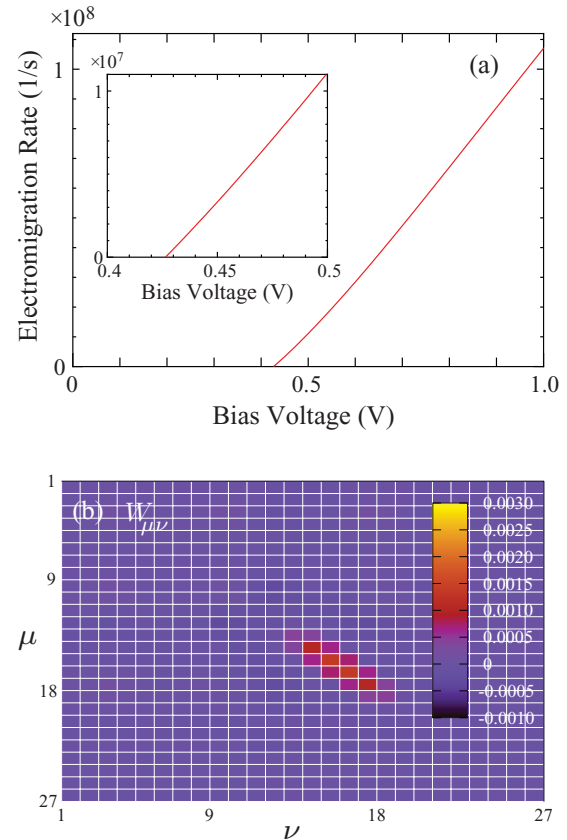


FIG. 3. (Color online) (a) Electromigration rate as a function of applied bias voltage. The inset shows the magnification around the threshold voltage. (b) Visual representation of the matrix  $\mathbf{W}$  at the lowest energy in the continuum states. In our calculations, a gold atom has nine orbitals, namely,  $6s$ ,  $6p_y$ ,  $6p_z$ ,  $6p_x$ ,  $5d_{xy}$ ,  $5d_{yz}$ ,  $5d_{3z^2-y^2}$ ,  $5d_{xz}$ , and  $5d_{x^2-y^2}$  in order. The matrix elements within orbitals 10–18 correspond to those of the migrating atom.

( $V_{\text{th}} \sim 0.42$  V). The monotonically increasing behavior can be expected from the form of Eq. (1), (4), or (5) because the electromigration rate depends explicitly on the width of the bias window. A magnified figure around  $V_{\text{th}}$  is given in the inset of Fig. 3(a). At the bias voltage  $V = V_{\text{th}}$ , the energy difference between the ionic ground state and the height of the lower barrier adjacent to  $\mathbf{R}_0$  in the inset of Fig. 1 is about 0.42 eV. This means that the nonadiabatic transition by ballistic electrons starts when the applied bias voltage becomes larger than the activation barrier of thermal migration at that bias.

The correlation between  $V_{\text{th}}$  and the activation barrier for thermal migration can be verified from a mathematical formulation. We consider no electronic excitation and no heat absorption in our calculations, namely, the electromigration rate in Eq. (5) has a finite value when  $f(E) - f(E + \varepsilon_0 - \varepsilon + eV) > 0$ , where  $E$ ,  $\varepsilon$ , and  $\varepsilon_0$  are the energies of electrons, the ionic continuum, and ground states, respectively. When the energy origin of the ionic states at each bias voltage is set to the top of the lower (left) barrier adjacent to  $\mathbf{R}_0$  in the inset of Fig. 1, then  $-\varepsilon_0$  can be basically considered as the barrier height of the thermal migration at each voltage,  $U_b(V)$ , and  $\varepsilon$  must be  $0 < \varepsilon < \varepsilon_0 + eV$  in order to meet the condition  $f(E) - f(E + \varepsilon_0 - \varepsilon + eV) > 0$ . This means that  $V_{\text{th}} = -\varepsilon_0(V_{\text{th}})/e \sim U_b(V_{\text{th}})/e$ . Therefore the electron-mediated excitations from the ionic ground state toward the continuum states are triggered above  $V_{\text{th}}$ .

To clarify the nature of the trigger of the nonadiabatic transition, the elements of the matrix  $\mathbf{W}$  represented in terms of electron atomic orbitals located over three atoms in Fig. 2 are given in Fig. 3(b). The orbital indices  $\mu$  and  $\nu$  with numbers in the range 10–18 indicate the atomic orbitals of the migrating atom. We observe from Fig. 3(b) that the matrix elements between orbitals on the migrating atom itself have larger values. The scattering potential for electronic transitions  $W_{\varepsilon \leftarrow \varepsilon_0}(\mathbf{r})$  in Eq. (3) is a short-ranged function because the atomic potential  $V(r)$  in Eq. (3) has a finite value within a few angstroms at most. As a result, the localized  $5d$  orbitals of the migrating atom are considerably overlapped with the  $W_{\varepsilon \leftarrow \varepsilon_0}(\mathbf{r})$  compared with the valence orbitals and the orbitals of the neighboring atoms, and the matrix elements of the  $5d$  orbitals become larger than the others. Although the presence of the density of states originating from the  $5d$  orbitals around the Fermi energy is a requisite condition, the trigger is the electronic scattering by the  $5d$  orbitals.

#### IV. CROSSOVER BETWEEN NONADIABATIC AND THERMAL MIGRATION

We have investigated the electromigration rate by thermal activation associated with Joule heating around the migrating atom.<sup>13</sup> It was found from previous work that the gold atom steadily migrates if the local temperature around the migrating atom is higher than room temperature. The previous results are summarized in Fig. 4. In the present work, we will focus on the voltage or temperature dependence of the nonadiabatic electromigration rate to discuss whether the nonadiabatic process is dominant or not compared with the thermal activation process.

We can clearly see in Fig. 4 that the thermal activation contribution to the electromigration rate at each voltage

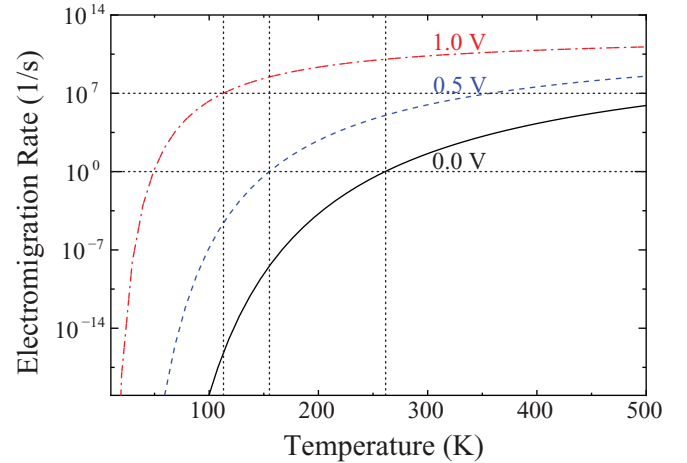


FIG. 4. (Color online) Electromigration rate by thermal activation associated with Joule heating around the migrating atom. The electromigration rates at 0.0, 0.5, and 1.0 V are depicted by the solid, dashed (blue), and dot-dashed (red) curves, respectively.

increases almost exponentially with temperature for a narrow temperature range. An increase of the voltage also strongly enhances the migration rate. Comparing the magnitude of the electromigration rate contributed nonadiabatically in Fig. 3 and by local heating in Fig. 4, we can find the crossover between the nonadiabatic and thermal migration regimes.

To clearly see the crossover, the nonadiabatic electromigration rates are given in Fig. 5, together with the electromigration rate via thermal activation. Figure 5(a) shows the electromigration rate at 0.5 V, which is a voltage slightly over  $V_{\text{th}}$  and

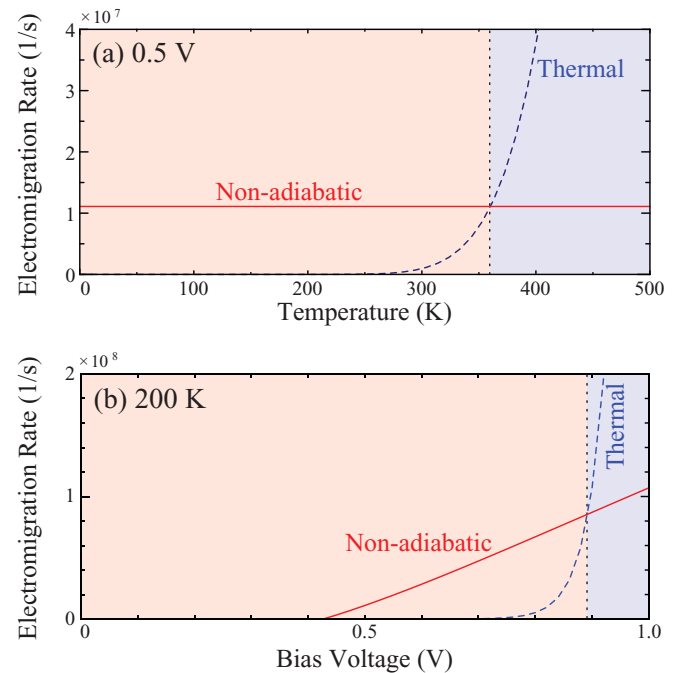


FIG. 5. (Color online) Nonadiabatic electromigration rates together with the electromigration rate via thermal activation at (a) 0.5 V and (b) 200 K. The solid (red) lines and dashed (blue) curves are the nonadiabatic and thermal contributions to the electromigration rates. The vertical dotted lines represent the thresholds.

experimentally intriguing, especially in nanogap formation by electromigration.<sup>6</sup> We observe the crossover at about 360 K in Fig. 5(a). Note that the nonadiabatic electromigration rate at any voltage is independent of temperature in the present formulation. An interesting finding is that the nonadiabatic contribution predominates even in the range somewhat over room temperature. Figure 5(b) represents the electromigration rate at 200 K. We can see that the crossover appears at 0.89 V, and the nonadiabatic contribution is dominant in this case. The above observations indicate that the nonadiabatic contribution has an advantage in electromigration at low temperature and low bias beyond  $V_{th}$ . Electromigration with nonthermal origin in gold junctions has been observed in recent experiments also.<sup>4,6</sup>

## V. SUMMARY AND OUTLOOK

Nonadiabatic electromigration of a gold atom along a one-dimensional gold chain was theoretically investigated. We observed that the calculated electromigration rate exhibits almost linear behavior, and a nonadiabatic transition via the electron wind starts when the applied bias voltage becomes larger than the activation barrier of thermal migration at

that bias. It is found that inelastic electronic scattering to a lower ballistic state, exciting vibrational states of the migrating atom, works to kick the atom and induces the migration. In this process the  $d$  orbitals with larger lobes in the migration direction play a dominant role. Furthermore, we compared the electromigration by nonadiabatic transitions with that by thermal activation and found the crossover between them. From the analysis of the crossover, we clarified that the nonadiabatic contribution becomes dominant at low temperature and low bias beyond  $V_{th}$ .

In this study, we considered nonadiabatic excitations from an ionic ground state only. In the next stage, we will treat multiple excitation and deexcitation processes. Our ultimate goal is to deal with both nonadiabatic and thermal electromigration on an equal footing and to simulate the process using calculated electromigration rates.

## ACKNOWLEDGMENTS

The authors thank Akinori Umeno and Kazuhiko Hirakawa for fruitful discussions. The computation in this work was performed in part at the Supercomputer Center, Institute for Solid State Physics, The University of Tokyo.

\*araidai@wpi-aimr.tohoku.ac.jp

†tsukada@wpi-aimr.tohoku.ac.jp

<sup>1</sup>R. S. Sorbello, *Solid State Phys.* **51**, 159 (1997), and references therein.

<sup>2</sup>C. Durkan and M. E. Welland, *Ultramicroscopy* **82**, 125 (2000).

<sup>3</sup>M. Hauschildt, M. Gall, S. Thrasher, P. Justison, L. Michaelson, R. Hernandez, H. Kawasaki, and P. S. Ho, *Appl. Phys. Lett.* **88**, 211907 (2006).

<sup>4</sup>Zhen Ming Wu, M. Steinacher, R. Huber, M. Calame, S. J. van der Molen, and C. Schönenberger, *Appl. Phys. Lett.* **91**, 053118 (2007).

<sup>5</sup>Zhen Ming Wu, Song Mei Wu, S. Oberholzer, M. Steinacher, M. Calame, and C. Schönenberger, *Phys. Rev. B* **78**, 235421 (2008).

<sup>6</sup>A. Umeno and K. Hirakawa, *Appl. Phys. Lett.* **94**, 162103 (2009).

<sup>7</sup>T. Kizuka, S. Kodama, and T. Matsuda, *Nanotechnology* **21**, 495706 (2010).

<sup>8</sup>M. Di Ventra, S. T. Pantelides, and N. D. Lang, *Phys. Rev. Lett.* **88**, 046801 (2002).

<sup>9</sup>M. Brandbyge, K. Stokbro, J. Taylor, J.-L. Mozos, and P. Ordejon, *Phys. Rev. B* **67**, 193104 (2003).

<sup>10</sup>S. Heinze, N.-P. Wang, and J. Tersoff, *Phys. Rev. Lett.* **95**, 186802 (2005).

<sup>11</sup>Y. Girard, T. Yamamoto, and K. Watanabe, *J. Phys. Chem. C* **111**, 12478 (2007).

<sup>12</sup>E. J. McEniry, D. R. Bowler, D. Dundas, A. P. Horsfield, C. G. Sánchez, and T. N. Todorov, *J. Phys.: Condens. Matter* **19**, 196201 (2007).

<sup>13</sup>M. Araidai and M. Tsukada, *Phys. Rev. B* **80**, 045417 (2009).

<sup>14</sup>C. Verdozzi, G. Stefanucci, and C.-O. Almbladh, *Phys. Rev. Lett.* **97**, 046603 (2006).

<sup>15</sup>M. Brandbyge, J.-L. Mozos, P. Ordejón, J. Taylor, and K. Stokbro, *Phys. Rev. B* **65**, 165401 (2002).

<sup>16</sup>T. Ozaki, K. Nishio, and H. Kino, *Phys. Rev. B* **81**, 035116 (2010).

<sup>17</sup>M. Elstner, D. Porezag, G. Jungnickel, J. Elsner, M. Haugk, Th. Frauenheim, S. Suhai, and G. Seifert, *Phys. Rev. B* **58**, 7260 (1998).

<sup>18</sup>As clearly seen in Eq. (3), adiabatic driving forces are reflected in the electromigration rate through the ionic states  $\Phi(\mathbf{R})$ , which are the solutions of the Schrödinger equation at the potential-energy surface of the migrating atom.

<sup>19</sup>J. H. Davies, *The Physics of Low-Dimensional Semiconductors* (Cambridge University Press, Cambridge, England, 1998).